Published in final edited form as:
Cell. 2008 December 26; 135(7): 1263–1275. doi:10.1016/j.cell.2008.11.020.

Real-time Visualization of Dynamin-catalyzed Membrane Fission and Vesicle Release

Thomas J. Pucadyil and **Sandra L. Schmid***
Department of Cell Biology, The Scripps Research Institute, La Jolla, CA 92037, USA

Abstract

The GTPase dynamin assembles at the necks of budded vesicles *in vivo* and functions in membrane fission. We have developed fluid supported bilayers with excess membrane reservoir, (SUPER) templates, to assay vesicle formation and membrane fission. Consistent with previous studies, in the absence of GTP, dynamin assembles in spirals forming long membrane tubules. GTP addition triggers disassembly, but not membrane fission arguing against models that fission is mediated by concerted and global GTP-driven conformational changes. In contrast, under physiological conditions in the constant presence of GTP, dynamin mediates membrane fission. Under these conditions, fluorescently-labeled dynamin cooperatively organizes into self-limited assemblies that continuously cycle at the membrane and drive vesicle release. When visualized at the necks of emergent vesicles, self-limited dynamin assemblies display intensity fluctuations and persist for variable time periods before fission. Thus, self-limited assemblies of dynamin generated in the constant presence of GTP catalyze membrane fission.

Keywords

Dynamin; supported bilayers; membrane reservoir; membrane fission; GTPase activity

INTRODUCTION

Vesicular transport and organelle biogenesis critically depend on membrane fission (Chernomordik and Kozlov, 2003). During endocytosis, membrane fission is a regulated process dependent on the GTPase dynamin (Conner and Schmid, 2003). Dynamin-1, the best-studied neuronal isoform, spontaneously self-assembles on favorable membrane templates to form helical spirals (Stowell et al., 1999; Sweitzer and Hinshaw, 1998), which appear similar to electron-dense collars found at the necks of arrested endocytic pits at the synapse of *shibire* flies (Kosaka and Ikeda, 1983).

Current models propose a mechanochemical role for dynamin in membrane fission. It is assumed that a concerted nucleotide-dependent conformational change such as a GTP binding-dependent constriction (Sweitzer and Hinshaw, 1998; Zhang and Hinshaw, 2001), hydrolysis-dependent longitudinal expansion (Stowell et al., 1999) or twisting (Roux et al., 2006) of a preassembled dynamin scaffold generates the force required to sever membranes. Importantly, these models suggest that dynamin alone is insufficient and that fission requires other factors

*Address correspondence to Sandra L. Schmid., E-mail: E-mail: SLSchmid@scripps.edu, Phone: 858-784-2311, FAX: 858-784-2345.

such as a clathrin coat (Stowell et al., 1999) or actin filaments (Itoh et al., 2005; Roux et al., 2006). A preassembled state of dynamin is unlikely to exist in cells because GTP hydrolysis causes its rapid disassembly and dissociation from the membrane (Warnock et al., 1996) resulting at steady state in the formation of dynamic, self-limited assemblies (Ramachandran and Schmid, 2008). Therefore, the relevance of GTP-dependent global conformational changes and/or preassembled dynamin scaffold dynamics to membrane fission remains unclear. Likewise, whether the dynamic, self-limited assemblies of dynamin formed in the presence of GTP on a membrane template can mediate fission is not known.

Analyzing dynamin behavior in the presence of GTP has been experimentally challenging due to the rapid kinetics of its membrane binding and dissociation. Furthermore, correlating previous models of dynamin organization and function to membrane fission is complicated by the absence of quantitative assays (Antonny, 2006). Fission, leading to the release of endocytic transport intermediates, has been studied using perforated cells and purified cell membranes (Schmid and Smythe, 1991; Miwako and Schmid, 2005). However, due to the biochemical complexity of these systems, the minimum machinery required for fission remains undefined. On the other hand, partial reconstitution of transport processes using semi-purified or purified coat and accessory proteins on protein-free liposomes have required electron microscopic (EM) analysis thereby offering limited temporal resolution to analyze reaction intermediates (Takei et al., 1998). Light scattering has been used in potentially quantitative assays for membrane fission (Sweitzer and Hinshaw, 1998; Yoshida et al., 2004), but changes in light scattering are difficult to interpret in heterogeneous mixtures. Indeed, recent evidence suggests that observed changes in light scattering reflect protein dissociation from the membrane and not membrane fission (Danino et al., 2004; Ramachandran and Schmid, 2008).

We have developed a novel model membrane system of negatively charged and fluid supported lipid bilayers with excess membrane reservoir on silica beads, potentially suitable for reconstitution of vesicular transport. A major advantage of this system is that it can be used interchangeably in real-time microscopy and quantitative biochemical assays allowing us to analyze dynamin behavior on a membrane template under the constant presence of GTP.

RESULTS

Supported bilayers with excess membrane reservoir (SUPER) as a novel template for vesicular transport

We first generated conventional supported bilayers using previously described methodologies (Galneder et al., 2001; Baksh et al., 2004). Silica beads suspended in water were incubated with increasing concentrations of liposomes whose composition approximately reflects that of the inner leaflet of plasma membranes in terms of net charge (Lemmon, 2008). The adsorbed liposomes rupture and fuse to form uniform bilayers around the beads and unbound liposomes are removed by subsequent washes. Liposome binding isotherms indicate that at saturation (Figure 1A), beads displayed fluorescence intensity equivalent to $2.5 \pm 0.1 \times 10^8$ lipid molecules/bead, in agreement with the expected number of 2.4×10^8 assuming a single bilayer deposited around a 5 μm sphere and a lipid cross-sectional area of 65 $Å^2$. Conventional supported bilayers are stable and lack excess reservoir. However, we found that when supported bilayers were prepared in high salt and subsequently washed with water to remove unbound liposomes and excess salt, each bead now displayed fluorescence intensity equivalent to $7.0 \pm 0.3 \times 10^8$ lipid molecules/bead, which reflects an ~3 fold increase in membrane reservoir. To distinguish these from conventional supported bilayers, we refer to them as supported bilayers with excess membrane reservoir, or SUPER templates.

We monitored the susceptibility of a membrane-incorporated fluorescent lipid probe NBD-PE to dithionite-mediated fluorescence quenching (McIntyre and Sleight, 1991) to determine

whether the excess membrane reservoir was indeed a bilayer. Addition of 5 mM dithionite caused quenching of NBD-PE fluorescence to ~50%, with kinetics similar to that seen with extruded liposomes indicating that SUPER templates are unilamellar (Figure 1B). When added to a drop of buffer on a glass coverslip, the excess membrane reservoir spilled out from the template and was visualized as a patch of membrane now adsorbed to the coverslip (Figure 1C, white arrows and Movie S1). Conventional supported bilayers did not show such a membrane spill (Figure 1D). Further, FRAP experiments established that the fluorescent lipid probe BODIPY FL C_{12}-HPC in supported bilayers prepared under high-salt conditions on glass coverslips exhibited an apparent diffusion coefficient of $2.2 \pm 0.7\ \mu m^2\ s^{-1}$ and a mobile fraction of ~100% (see Figure S1), confirming the fluidity of lipids in SUPER templates.

SUPER templates were further characterized by membrane tether pulling experiments. Membrane tethers could be easily pulled to several tens of microns in length without undergoing rupture (Figure 1E, Movie S2). The fluorescence intensity along the tether remained uniform during tether extension further indicating that the membrane around these templates is unilamellar. Tethers pulled from SUPER templates did not appear taut; instead they swayed gently (see Movie S2). Based on the premise that during extension, a build-up of tension over that already existing in the membrane would cause thinning (and hence a drop in fluorescence) of tethers, we analyzed the integrated fluorescence at a fixed region of interest (ROI) as it was extended. No significant decline in fluorescence was apparent even when tethers were extended up to 30 μm (Figure 1F). Interestingly, tether fluorescence showed an increase upon retraction (Figure 1F) and became thicker and more flaccid as it got closer to the bead (see Movie S2). This is possibly due to the speed of retraction not allowing the tether to be taken back completely into the template. As expected, we were unable to pull tethers from SUPER templates that had spilled their excess membrane reservoir on a glass surface (as in Figure 1C). Taken together, SUPER templates represent a novel supported bilayer system that possesses a large fluid reservoir of unilamellar membranes readily accessible to external manipulations.

Dynamin-induced membrane tubulation on SUPER templates

We first monitored the effect of dynamin on Rhodamine-PE- (RhPE) containing SUPER templates in real-time using fluorescence microscopy. Templates were added to 100 μl buffer placed on a coverslip and allowed to settle. The coverslip was pre-coated with PEG-silane to prevent binding and spillover of the excess membrane reservoir. Dynamin was added from a stock solution at the side and allowed to diffuse slowly into the buffer to achieve a final concentration of 0.5 μM. Addition of dynamin led to the growth of numerous membrane tubules from the templates (Figure 2A, yellow arrows and Movie S3), with the bead taking on a ‘hairy’ appearance. Tubules grew to several microns in length and displayed heterogeneity in fluorescence. Initially faint tubules (Figure 2A, yellow arrows) growing from adjacent beads encountered each other, became intertwined and tethered between the templates to form thicker, brighter structures (Figure 2A, white arrow). Dynamin-dependent tubulation in this system, as in others (Stowell et al., 1999; Roux et al., 2006; Ramachandran and Schmid, 2008), required the presence of PI-4,5-P_2 in the membrane (data not shown). Fluorescent BODIPY-labeled dynamin (BODIPY-dynamin) (Ramachandran et al., 2007), although enriched on these tubules is also found on the relatively planar bead surface (Figure 2B,C).

Negative-stain EM of SUPER templates incubated with dynamin showed that the bundles of membrane tubules seen using fluorescence microscopy (Figure 2A) are in fact coiled membrane tubules (Figure 2D and 2E). This is reminiscent of the microtubule bundling property originally reported for dynamin (Shpetner and Vallee, 1989) and suggests that lateral interactions can occur between assembled dynamin scaffolds. Individual membrane tubules showed a scaffold with an outer diameter of 45.5 ± 5.0 nm (mean ± SD, n=19) and a

characteristic striated appearance (Figure 2F). Taken together, these results indicate that SUPER templates respond to dynamin in a manner similar to conventional membrane templates like liposomes.

Real-time observation of dynamin-catalyzed membrane fission

Dynamin has been ascribed a GTP-dependent mechanochemical role in membrane fission (Sweitzer and Hinshaw, 1998; Stowell et al., 1999; Roux et al., 2006). However, in each of these studies dynamin was preassembled on a membrane template before adding GTP. Indeed, the behavior of dynamin on a membrane template has not been observed in the presence of GTP, a more physiologically relevant condition. We therefore added dynamin to SUPER templates bathed in buffer containing 1 mM GTP. Under these conditions, we did not detect tubule formation. Instead, addition of dynamin led to the continuous release of numerous vesicles diffusing randomly in solution (Figure 3A, yellow arrows and Movie S4). Similar experiments performed in the presence of a non-hydrolyzable GTP analogue, GMPPCP or GDP led to the growth of shorter membrane tubules without release of vesicles (data not shown). Vesicle release in the presence of GTP is apparent from the cumulative increase in fluorescence intensity of the bathing solution (Figure 3B and Movie S4), which was not observed with dynamin alone or in the presence of GMPPCP or GDP (Figure 3B).

Negative stain EM of the bathing solution in the presence of dynamin and GTP confirmed the presence of lipid vesicles (Figure 3C, black arrows), with an estimated size of 74 ± 33 nm (mean±SD, n=221) (Figure 3D). No vesicles were observed in the absence of GTP (Figure 3C, inset). The dark, negatively stained structures detected under both conditions probably correspond to small dynamin aggregates. These data show that dynamin alone is sufficient to catalyze membrane fission and vesiculation from a fluid membrane reservoir.

Dynamin behavior during membrane fission

We monitored the behavior of Alexa Fluor 488-labeled dynamin (Ax488dyn) added to SUPER templates in the presence of GTP. Diffusion of Ax488dyn into the field coincides with the appearance of fluorescent puncta most easily detected at the periphery of the bead (Figure 4A, yellow arrows and Movie S5). Such a distribution of dynamin coincided with punctate, though less pronounced, RhPE fluorescence (Figure 4B, yellow arrows), which could represent short membrane tubules/buds formed as dynamin self-assembles on the membrane. Dynamin assemblies displayed fluctuations in fluorescence intensity that could reflect multiple rounds of assembly and disassembly (see Movie S5). These structures could represent intermediates in the fission process, which eventually produces vesicles from SUPER templates as seen in Figure 3A. With time, freely diffusing punctate dynamin fluorescence appeared in the bathing solution (Figure 4A, red arrows and Movie S5) and colocalized with RhPE (Figure 4C, yellow arrows). These results suggest that small tubules/buds, formed due to dynamin self-assembly on the template, undergo fission and are released as vesicles. If so, in the presence of GTP, continuous cycling of such events should maintain a steady state distribution of dynamin on the template and at the same time result in progressive depletion of the membrane reservoir. Quantitative analysis of Ax488dyn and RhPE fluorescence on individual beads (n=8) (Figure 4D) under these conditions indeed showed a continuous decline in the membrane reservoir while dynamin remained at steady state.

Biochemical analysis of membrane fission

SUPER templates dispersed in solution can be pelleted by a low speed spin allowing us to unambiguously monitor membrane fission and vesicle release using a simple sedimentation assay (Figure 5A). After incubation of RhPE-labeled supported bilayers with buffer for 30 min at 25°C and sedimentation, a small level of fluorescence (~4% of total) could be detected in the supernatant. This background corresponds to unbound liposomes still present after

preparation of templates, as a similar level was detected after resedimentation of the stock solution of templates. There was no increased release of RhPE over background when templates were incubated in buffer containing dynamin alone, or in the presence of GDP or GMPPCP. Importantly, incubation of templates with buffer containing dynamin and GTP caused a significant (~5 fold) increase in RhPE release (~20% of total). The nucleotide dependence for fission seen with the microscopy-based assay (Figure 3) corresponded to that seen in the sedimentation assay (Figure 5A), establishing its validity. This quantitative assay was therefore used to explore the requirements for dynamin-catalyzed membrane fission.

The extent of membrane fission displayed a linear dependence on dynamin concentration above 0.1 μM (Figure 5B). Given that dynamin shows a high degree of cooperativity in binding and self-assembly in the absence of GTP (Stowell et al., 1999), this linearity suggests that the presence of GTP regulates dynamin assembly to a critical number of molecules capable of mediating fission (seen in Figure 4A). These assemblies would remain constant in size but increase in abundance with an increase in protein concentration. The lack of significant fission at 0.1 μM could reflect its low membrane binding affinity and consequently reduced self-assembly on the membrane. The extent of membrane fission was also linearly dependent on the template concentration (Figure 5C). Membrane fission showed a linear increase with time (Figure 5D), although we observed burst phase kinetics at early time points (initial 10 min) (Figure 5D). At steady state, the rate of fission in the presence of 0.25 μM dynamin was 0.08 ±0.01% total min^{-1} (mean±SD, n=3), which approximately doubled to 0.19±0.02% total min^{-1} (mean±SD, n=3) in the presence of 0.5 μM dynamin. GTP hydrolysis occurred at a constant rate of 3.0±.09 min^{-1} (mean±SD) in the presence of SUPER templates, which was ~40 fold higher than dynamin's basal GTPase activity of 0.08 ± 0.01 min^{-1} (mean±SD) (Figure 5E). Furthermore, the extent of membrane fission was linearly dependent on the PI-4,5-P_2 density in the membrane (Figure 5F).

The GTP-binding and self-assembling activities of dynamin were an absolute requirement for membrane fission. The S45N mutant, which is defective in GTP binding and inhibits clathrin-mediated endocytosis *in vivo* (Damke et al., 2001; Marks et al., 2001), was unable to catalyze membrane fission (Figure 5G). However, it could effectively inhibit the fission activity of wild type dynamin (Figure 5H). Since S45N can bind and tubulate SUPER templates even in the presence of GTP (see Movie S6), the inhibition by S45N could be due to coassembly with wild type dynamin to interfere with the latter's fission activity (Figure 5D). The R399A mutant displays a severe defect in quaternary structure in solution and on membranes (Ramachandran et al., 2007). As expected, no detectable membrane tubulation was observed with R399A (Movie S7), nor was R399A capable of mediating membrane fission (Figure 5G). Consistent with its reduced ability to bind and self-assemble on membranes, R399A was also unable to inhibit fission catalyzed by wild type dynamin (Figure 5H). Together, our biochemical assays establish that dynamin alone can catalyze membrane fission and vesicle formation from SUPER templates in a manner dependent on GTP binding, hydrolysis and regulated self-assembly.

Behavior of preassembled dynamin in presence of GTP

Previous studies of dynamin-dependent membrane remodeling events have involved the preassembly of dynamin spirals in the absence of nucleotides. We therefore also examined the effects of nucleotides on dynamin preassembled on SUPER templates. As previously shown (Figure 2), addition of Ax488dyn to SUPER templates led to the formation of dynamin-coated membrane tubules interconnecting the beads and forming an apparent network (Figure 6A, white arrows). Addition of GTP at this stage led to a rapid decrease in dynamin fluorescence on the templates (Figure 6A and Movie S8), with no significant change in RhPE fluorescence. Quantitative analysis of Ax488dyn and RhPE fluorescence on individual beads (n=8) showed

that GTP addition causes a rapid ($t_{1/2}$ ~1 sec) decline in dynamin fluorescence without a concomitant decrease in RhPE (Figure 6B), a kinetic trace quite different from that seen in the constant presence of GTP (Figure 4D).

Nonetheless, GTP addition caused rapid contraction of the membrane tubules drawing the templates closer together (see Movie S8). We analyzed the reason for this effect by examining bundled membrane tubules in greater detail (Figure 6C, white arrow). We find that GTP addition results in local increases in membrane density along the tubule (Figure 6C, yellow arrows and Movie S9). The appearance of these varicosities is consistent with GTP-dependent dissociation of the dynamin scaffold detected spectroscopically using fluorescently-labeled dynamin (Ramachandran and Schmid, 2008) and localized puckering of the lipid tubule detected by cryo-EM (Danino et al., 2004). This was followed by a rapid contraction of the tubule drawing the templates closer together (see Movie S9) and accumulation of membranes at the ends of the tubule (Figure 6C, red arrows). Tubules eventually underwent retraction and breakage. Then after a delay of several seconds, vesicle formation from templates resumed, although with much reduced efficiency (see Movie S9). These data suggest that after prolonged incubation in the absence of GTP, preassembled dynamin is kinetically trapped in an inactive state. Monitoring fluorescently-labeled dynamin under these conditions indeed shows that the retraction of the membrane tubule (Figure 6C) is due to partial disassembly and collapse of the dynamin scaffold (Figure 6D, yellow arrows and Movie S10). Following retraction, dynamin accumulates as large aggregates at the base of the membrane tubule (Figure 6D, red arrows), perhaps reflecting a kinetically trapped state. We also note that the addition of GMPPCP instead of GTP to bundled tubules (Figure S2, white arrow) caused the release of fainter tubules (Figure S2, yellow arrows) through a series of rotations suggesting uncoiling (see Movie S11). Thus, lateral interactions between assembled dynamin tubules appear to be disrupted by GTP binding.

Sedimentation assays also indicate a severe reduction in fission efficiency when GTP is added to preassembled dynamin. Thus, GTP addition to dynamin, preassembled on templates for 10 min, showed a dramatic reduction in both the kinetics and extent of membrane fission (Figure 6E). This inhibitory effect was time-dependent, presumably because at longer time points preassembly led to progressive growth and coiling of dynamin-coated membrane tubules (Figure 6F). From these data, we conclude that preassembled dynamin is not competent for fission.

Visualizing dynamin-catalyzed membrane fission

Although beyond our limits of resolution, dynamin-catalyzed fission events reconstituted in the presence of GTP on SUPER templates (Figures 3 and 4) most likely involve formation of a short membrane tubule, whose effective length is limited by both GTP hydrolysis-dependent dynamin disassembly and/or membrane fission. During the course of our experiments, we discovered conditions that could allow us to more clearly visualize the behavior of dynamin on longer tubular templates. The fluidity of the membrane reservoir was such that the viscous drag caused by the local addition of glycerol (50%) to SUPER templates caused a transient extension of the reservoir in the form a tube, which retracted as the glycerol equilibrated (final concentration 2%, see Figure S3). When dynamin was present in the glycerol solution, the membrane reservoir never extended out as a wide, floppy tube (Figure S3) but was rapidly constricted to form a long neck (Figure 7A, yellow arrows) that terminated in a bud (Figure 7A, white arrows) and remained tethered to the template (Figure 7A, yellow arrows and Movie S12). Such constricted buds were formed in several preparations of SUPER templates and were estimated to be 1.5±0.3 μm (mean±SD, n=77) in size (Figure 7B). When similar experiments were performed on SUPER templates bathed in buffer containing GTP, only short, neck-like regions of constriction were observed (Figure 7C, yellow arrows) often generating structures resembling beads-on-a-string with two (or more) necks (Figure 7C, white arrows and Movie

S13). These structures persisted for variable time periods before undergoing fission at one or other of the necks. In the example shown in Figure 7C, fission occurs first at the neck proximal to the bead (Figure 7C, red arrow and Movie S13) releasing a vesicle composed of conjoined buds. Importantly, this structure (Figure 7D), now completely detached from the template and diffusing freely in solution, undergoes fission at the neck (Figure 7D, white arrow) to release two vesicles (Figure 7D, red arrows and Movie S14). In the presence of GMPPCP or GDP, buds remained tethered with short membrane tubules at the neck without undergoing fission and release as vesicles (data not shown).

We monitored the distribution of BODIPY-dynamin on these structures to resolve finer details of the fission process. The initial flow of dynamin and glycerol induced bulging of the template, which was rapidly transformed into a bud with a constricted neck (Figure 7E, yellow arrows, Movie S15) that coincided with the localized assembly of BODIPY-dynamin (Figure 7E, red arrows). The entire bud/vesicle also showed diffuse staining with BODIPY-dynamin allowing us to simultaneously track the dynamics of the bud/vesicle and dynamin during fission. Even at early time points, dynamin fluorescence was higher around the neck presumably forming a collar-like structure (Figure 7E, red arrow in inset of the 1.4 s frame), indicating a propensity to assemble in a highly cooperative manner. This behavior is consistent with the early appearance of fluorescent speckles of dynamin on the surface of beads (Figure 4A). A well-defined constriction coincided with a localized increase in dynamin fluorescence around the neck (Figure 7E, red arrow in the 8.6 s frame). Even in the presence of GTP, the bud remained connected to the template through the neck for long periods (tens of seconds) before its release as a vesicle (Figure 7E, green arrow and Movie S15). Although the neck persisted, we observed fluctuations in dynamin fluorescence intensity (Figure 7F, red curve), significantly above those associated with the bud moving in and out of focus (Figure 7F, blue curve). Such fluctuations, which resembled the speckling behavior of fluorescent dynamin previously described to occur on the bead surface (Figure 4A), were observed in several examples of fission of large buds (see Figure S4) and are likely to reflect multiple assembly and disassembly cycles of dynamin occurring in the presence of GTP. We also noticed punctate dynamin fluorescence on the SUPER template and the bud (Figure 7E, white arrows and see Movie S15) similar to those observed when dynamin was added to templates without glycerol (Figure 4A) implying that the manner of dynamin addition (with or without glycerol) does not affect the steady state distribution of dynamin on the bead.

To rule out a possible complication in interpreting fission of large buds as being modulated by or a consequence of the flow of glycerol, we also analyzed the effect of dynamin addition to membrane tethers formed from SUPER templates in the presence of GTP. We focused on membrane tubules that were partially retracted and hence more flaccid (Figure 7G, white arrows and Movie S16) to simulate a system of free standing, untethered membrane templates. Strikingly, the addition of dynamin to such tubes caused fission at multiple sites, which occurred over the entire length of the tubes, and continued after the tube was severed, thus ultimately transforming it into small vesicles that diffused away into solution (Figure 7G, yellow arrows and Movie S16). These fission events occurred randomly along the length of the tube highlighting a stochastic nature of the fission process. Taken together, our results establish that dynamin and GTP are both necessary and sufficient to catalyze membrane fission.

DISCUSSION

We have developed a model membrane system of fluid supported bilayers on silica beads, refered to as SUPER templates, that allows us to both visualize and biochemically quantify dynamin-catalyzed membrane fission under physiological conditions in the constant presence of GTP. Previous models for dynamin-catalyzed membrane fission, based on the behavior of dynamin spirals preassembled in the absence of GTP, have suggested that global and concerted

conformational changes (*i.e.* constriction, helical expansion, twisting) upon GTP addition generate mechanochemical forces needed to drive membrane fission (Hinshaw and Schmid, 1995; Sweitzer and Hinshaw, 1998; Takei et al., 1998; Stowell et al., 1999; Roux et al., 2006). Our data are not consistent with these models. First, we find that preassembled dynamin scaffolds are not fission competent. If membrane fission was driven by a concerted GTP hydrolysis-dependent mechanical force, then GTP addition to preassembled dynamin should have favored fission events along the length of the tubule, which we did not observe. Rather, GTP addition triggered membrane dissociation, scaffold disassembly and tubule retraction without undergoing fission to release small vesicles. Indeed, our data suggest that preassembled dynamin structures may represent kinetically trapped, off-pathway intermediates.

The GTP-induced breakage of preassembled dynamin-coated membrane tubules tethered between templates shows striking similarity to recent DIC light microscopic analyses (Roux et al., 2006). These authors suggested that membrane fission was mediated by the GTPase-driven twisting of dynamin around the membrane tubule (Roux et al., 2006). However, breakage/fission was observed only when the membrane tubules were tethered by anchoring at one end or when the tubule was held taut by kinesin motors. Thus, it was suggested that dynamin alone could not drive fission and that externally applied membrane tension was necessary. Our data suggest two alternate explanations for these observations. First, since coiling reflects an intrinsic property of dynamin-coated membrane tubules, it may be that the GTP-dependent rotational dynamics of preassembled dynamin scaffolds observed by DIC (Roux et al., 2006) reflects uncoiling and retraction of these bundled tubules. Alternatively, the rotation may be due to localized expansion and dissociation of assembled dynamin from the lipid template. Since membrane tension has not been measured in either system, we cannot rule out that differences in intrinsic membrane tension in the templates described in Roux et al., 2006 and in SUPER templates might also contribute to these disparities. Regardless, our findings suggest that dynamin can catalyze membrane fission without the need to anchor the template.

Our data, and that of Bashkirov et al. (manuscript submitted) suggest that the primary response generated upon GTP hydrolysis in preassembled dynamin is its dissociation from the membrane without concomitant fission. In this scenario, addition of GTP to preassembled dynamin would cause retraction of the membrane tubule due to a weakening and disassembly of the dynamin scaffold. Consequently, membrane tubules tethered at both ends would break as a result of their undergoing retraction, an event that we believe does not reflect *bona fide* membrane fission because tubules undergo rupture in a region depleted of dynamin (compare Figure 6C and D and Movies S12 and S13). These results are in sharp contrast to the self-limited and localized assembly of dynamin seen in the presence of GTP that catalyzes membrane fission and vesicle release (Figure 4A and 7E).

Dynamin-catalyzed membrane fission required both its ability to bind and hydrolyze GTP and its ability to self-assemble. Self-assembly stimulates its GTPase activity, which in turn causes release of dynamin from the membrane (Danino et al., 2004; Ramachandran and Schmid, 2008). The presence of GTP *in vivo* would therefore be expected to maintain dynamin as a self-limited assembly on the membrane, reflecting a balance between spontaneous assembly and GTP hydrolysis-dependent disassembly, as is observed in the present case. On the SUPER template, such assemblies are likely to represent short membrane tubules that dynamically form, disassemble, and/or undergo fission. In the minimal reconstituted system described here, dynamin therefore appears to generate its own ‘neck’ and catalyze fission thereby releasing small vesicles. The homogeneity in vesicle sizes (~60–80 nm) further supports the notion that rather than mediating fission of preexisting buds, which would be variable in size, dynamin acts on self-generated tubular templates.

Our results indicate that dynamin-catalyzed membrane fission must involve a mechanism intrinsic to its self-assembly and disassembly cycles. Consistent with this model, it was recently shown by conductance measurements on membrane tubules, that dynamin self-assembly can force bilayers to come within critical proximity of each other such that the curvature stress imposed on the membrane bilayer could lead to spontaneous membrane fission (Bashkirov et al. ms submitted). Indeed, when added in the presence of GTP, dynamin induces stochastic fission of these tubules. In contrast, and consistent with our findings, addition of GTP to preassembled dynamin results in a relaxation of dynamin-induced curvature stress, consistent with disassembly, prior to membrane fission.

Is this potential mechanism of membrane fission unique to dynamin? We note that the Sar1 GTPase, which mediates COPII vesicle formation at the ER, can also generate curvature in membranes in the absence of GTP hydrolysis (Lee et al., 2005; Bielli et al., 2005). Its assembly is restricted to the necks of budding COPII vesicles as a result of the combined GEF activity of the ER-localized Sec12 that converts it into the GTP-bound, membrane-active form and the GAP activity of the COPII coat that causes membrane dissociation (Sato and Nakano, 2008). The assembly of the membrane curvature-inducing Arf1 GTPase (Beck et al., 2008), which mediates COPI vesicle formation at the Golgi, could similarly be localized to the neck through regulation by its Golgi-localized GEF, GBF1 (Gillingham and Munro, 2007) and ArfGAP1, whose activity is stimulated by positive curvature of a small bud (Bigay et al., 2003). Thus, it is possible that the paradigm of local generation of high curvature and dynamic interactions of membrane curvature-generating scaffolds at these sites might be a general mechanism of membrane fission during vesicle formation. Dynamin is distinct from these GTPases because it does not require a GEF for membrane binding and has an intramolecular, assembly-dependent GAP that allows it to function as a minimal fission apparatus whose dynamic behavior and restricted assembly at sites of fission are intrinsically regulated by cycles of GTP binding and hydrolysis.

It is likely that even in a complex cellular environment, dynamin would display a similar potential for catalyzing membrane fission. Indeed, our observations of the speckling behavior of dynamin on a membrane surface and the appearance and disappearance at the necks of budding vesicles are consistent with the transient recruitment of dynamin to coated pits observed by total internal reflection microscopy and its coincident disappearance along with vesicle release (Merrifield et al., 2002), although the kinetics of fission *in vivo* are significantly faster. Thus, although dynamin alone is sufficient to catalyze fission, it is likely that coats and other accessory proteins increase the efficiency of fission. Dynamin partners and coat components might function to spatially and temporally localize dynamin assembly/disassembly at sites of vesicle formation and fission and/or to generate or stabilize curvature at the neck region. Endocytic accessory factors might also function to apply external tension enhancing the efficiency of dynamin-catalyzed fission, as has been suggested (Roux et al., 2006). Further studies will be needed to identify and address the potential role(s) of endocytic accessory proteins in dynamin-catalyzed membrane fission. Importantly, the SUPER template we have developed provides a powerful means to measure and visualize these events in a biochemically-defined system. The successful reconstitution of dynamin-catalyzed membrane fission under a more physiologically relevant scenario emphasizes the potential applicability of reconstituting several other forms of vesicular transport using the SUPER template.

EXPERIMENTAL PROCEDURES

Preparation of Liposomes and SUPER Templates

1,2-dioleoyl-*sn*-glycero-3-phosphocholine (DOPC), 1,2-dioleoyl-*sn*-glycero-3-(phospho-L-serine) (DOPS), triammonium salt of porcine brain L-α-phosphatidylinositol-4,5-bisphosphate (PI-4,5-P_2) and 1,2-dioleoyl-*sn*-glycero-3-phosphoethanolamine-*N*-(Lissamine Rhodamine B

Sulfonyl) (RhPE) were from Avanti Polar Lipids. Stock solutions of phospholipids were aliquoted into a glass tube and the solvent was dried rapidly under a stream of nitrogen while being warmed gently (~50°C). Lipids were further dried under hard vacuum for 1 hr and hydrated in 20 mM Hepes pH 7.5, 150 mM NaCl buffer for 1 hr at 37°C with intermittent vortexing. Multilamellar vesicles thus produced were subjected to multiple freeze-thaw cycles using liq. N_2 before being extruded through 100 nm polycarbonate filters using an Avanti Mini-extruder to generate unilamellar vesicles. Silica beads (5 μm diameter, Corpuscular Inc., typically 5×10^6) and unilamellar vesicles (final concentration=200 μM) were mixed in a total volume of 100 μl of 20 mM Hepes pH 7.5, 600 mM NaCl buffer in a polypropylene centrifuge tube, and incubated for 30 min at 25°C with intermittent vortexing. Beads were subsequently washed with deionized water by pulse vortexing and sedimenting at low speed (260 *g*) for 2 min at 25°C in a swinging bucket rotor. The lipid concentration in a routine preparation of templates was 58±3 μM (mean±SD).

Fluorescence Spectroscopy and Dithionite Quenching Experiments

Fluorescence intensity of liposomes and SUPER templates containing 2 mol% NBD-PE (Invitrogen) and SUPER templates made from such liposomes was recorded before and after adding 10 μl of 1 M dithionite (Sigma) stock solution prepared in 1 M Tris pH 10.0 buffer, while being continuously stirred. Fluorescence intensities were acquired in a Fluorolog-3 steady-state spectrofluorometer (Horiba Jobin Yvon) at excitation and emission wavelengths of 470 nm (2 nm bandpass) and 540 nm (4 nm bandpass), respectively, in a temperature-controlled 1 cm × 1 cm quartz cuvette at 25 °C. All experiments were performed in 20 mM HEPES, pH 7.5, 150 mM NaCl buffer containing 10 μM unlabeled DOPC liposomes in order to prevent SUPER templates from binding and spilling their excess reservoir on to the walls of the cuvette.

Membrane Tether Pulling Experiments

Membrane tethers were pulled from SUPER templates deposited on BSA-coated glass coverslips in 20 mM HEPES pH 7.5, 150 mM NaCl buffer using a 5 μm carbon fiber (ALA Scientific Instruments) attached to a Nano-PZ piezomicromanipulator (Newport). Tethers were imaged on an Olympus IX-70 microscope using a 150X, 1.45 NA oil-immersion objective equipped with a Cascade-II CCD camera (Photometrics). Tether fluorescence intensities (plotted in Figure 1F) were calculated at a fixed ROI on the tether by fitting the fluorescence intensity profile across the tether to a Gaussian area function.

Dynamin Purification, GTPase Assays and Fluorescent Labeling

Dynamin 1 (wt and mutants) were expressed and purified as previously described (Leonard et al., 2005). Dynamin GTPase assay was carried out as described earlier (Leonard et al., 2005). Dynamin (0.5 μM) and GTP (1 mM) were premixed in 20 mM HEPES pH 7.5, 150 mM KCl, 1 mM $MgCl_2$ buffer at 25°C. The assay was started by adding SUPER templates and stopped by adding EDTA (final concentration=100 mM). Dynamin was conjugated to the thiol-reactive BODIPY Fl C1-IA (Invitrogen) or Alexa Fluor 488 C_5 maleimide (Invitrogen) probes as previously described (Ramachandran et al. 2007). Stoichiometry of labeling was 1:1 protein:dye (mol:mol) for BODIPY-dynamin and 1:2 protein:dye (mol:mol) for Alexa488-dynamin. BODIPY-dynamin and Alexa 488-dynamin were mixed with unlabeled dynamin at a 3:2 and 1:9 molar ratio respectively.

Fluorescence Microscopy

SUPER templates (typically 5×10^5) were imaged on PEG-silane (Gelest Inc.) coated glass coverslips (Fisher Scientific) in 100 μl of 20 mM HEPES pH 7.5, 150 mM KCl, 1 mM $MgCl_2$ buffer containing an oxygen scavenging system [50 μg/ml glucose oxidase (Sigma),

10 μg/ml catalase (Roche), 22.5 mM glucose (Sigma), and 1 mM DTT]. Dynamin stock solutions were applied to the edge of the drop of buffer and allowed to diffuse. Assays typically contained final concentrations of 0.5 μM dynamin and 1 mM nucleotides (Sigma or Jena Bioscience GmbH). Fluorescence imaging was carried out at 25°C on an inverted Olympus IX-70 microscope using a 100X, 1.35 NA oil-immersion objective and equipped with a CH350L CCD camera (Photometrics) with 490/20 nm excitation and 528/38 nm emission filters for Alexa Fluor 488- or BODIPY-labeled dynamin and 555/28 nm excitation and 617/73 nm emission filters for RhPE-labeled membranes. Dual-color microscopy was carried out on a Nikon TE2000U microscope using a 60X, 1.45 NA oil-immersion objective equipped with a Cascade II CCD camera (Photometrics), 50 mW KrAr laser source (Melles Griot) and a Dual-View (525/30 nm, 620/50 nm bandpass filters with a 565 nm dichroic filter) (Optical Insights). FRAP on supported bilayers was performed at 25°C on a Bio-Rad Radiance 2100 Rainbow confocal microscope attached to a Nikon TE2000-U using a 60X, 1.4NA oil-immersion objective. Images were analyzed and compiled using ImageJ (http://rsb.info.nih.gov/ij/).

Sedimentation Assays

SUPER templates (typically 5×10^5) were suspended in 100 μl of 20 mM Hepes pH 7.5, 150 mM KCl, 1 mM $MgCl_2$ buffer ± dynamin ± nucleotides in a 0.5 ml polypropylene centrifuge tube at 25 °C. Tubes were spun at low speed (260 *g*) at 25 °C in a swinging bucket rotor. 75 μl of the supernatant was removed and mixed with 25 μl of 0.4% Triton X-100. Total membrane fluorescence on the beads (Total) was estimated in a separate reaction by adding templates to 0.1% Triton X-100. Fluorescence intensity of the supernatant was read in a 96 well plate reader (Bio-Tek Instruments) at 25 °C using 530/25 nm excitation and 590/25 nm emission filters.

Negative Staining and Electron Microscopy

To analyze dynamin assembly, SUPER templates were added to assay buffer containing 0.5 μM dynamin and incubated for 30 min at 25 °C. Sample aliquots (3–5 μl) were spotted on a copper grid and left for 5 min. Excess buffer was blotted and samples were stained with 1% uranyl acetate. Excess stain was washed off with water. To analyze the supernatant of a fission reaction, templates were added to assay buffer containing 0.5 μM dynamin ± 1 mM GTP, incubated for 30 min at 25 °C, and spun down. Aliquots (3–5 μl) of the supernatant were spotted on a glow discharged copper grid and left for 5 min. Samples were stained as described above. Transmission electron micrographs were acquired on a Philips CM100 electron microscope equipped with a Mega View III CCD camera (Olympus Soft Imaging Systems) and analyzed and compiled using ImageJ.

Supplementary Material

Refer to Web version on PubMed Central for supplementary material.

Acknowledgements

We acknowledge Malcolm R. Wood for help with electron microscopy, Vadim Frolov for help with the membrane tether pulling experiments, and Sharmistha Acharya and Marilyn Leonard for technical assistance. We thank William Balch, Vadim Frolov, Shanti Kalipatnapu, Allen Liu, Rajesh Ramachandran and Joshua Zimmerberg for discussions and critical comments on the manuscript. This work is supported by grants from NIH to S.L.S (R01.GM042455 and R37.MH61345). T.J.P. is a fellow of The Leukemia and Lymphoma Society. This is TSRI manuscript no. 19489.

References

Antonny B. Membrane deformation by protein coats. Curr Opin Cell Biol 2006;18:386–394. [PubMed: 16782321]

Baksh MM, Jaros M, Groves JT. Detection of molecular interactions at membrane surfaces through colloid phase transitions. Nature 2004;427:139–141. [PubMed: 14712272]

Beck R, Sun Z, Adolf F, Rutz C, Bassler J, Wild K, Sinning I, Hurt E, Brügger B, Béthune J, Wieland F. Membrane curvature induced by Arf1-GTP is essential for vesicle formation. Proc Natl Acad Sci USA 2008;105:11731–11736. [PubMed: 18689681]

Bigay J, Gounon P, Robineau S, Antonny B. Lipid packing sensed by ArfGAP1 couples COPI coat disassembly to membrane bilayer curvature. Nature 2003;426:563–566. [PubMed: 14654841]

Chernomordik LV, Kozlov MM. Protein-lipid interplay in fusion and fission of biological membranes. Annu Rev Biochem 2003;72:175–207. [PubMed: 14527322]

Conner SD, Schmid SL. Regulated portals of entry into the cell. Nature 2003;422:37–44. [PubMed: 12621426]

Damke H, Binns DD, Ueda H, Schmid SL, Baba T. Dynamin GTPase domain mutants block endocytic vesicle formation at morphologically distinct stages. Mol Biol Cell 2001;12:2578–2589. [PubMed: 11553700]

Danino D, Moon KH, Hinshaw JE. Rapid constriction of lipid bilayers by the mechanochemical enzyme dynamin. J Struct Biol 2004;147:259–267. [PubMed: 15450295]

Galneder R, Kahl V, Arbuzova A, Rebecchi M, Rädler JO, McLaughlin S. Microelectrophoresis of a bilayer-coated silica bead in an optical trap: application to enzymology. Biophys J 2001;80:2298–2309. [PubMed: 11325731]

Gillingham AK, Munro S. The small G proteins of the Arf family and their regulators. Ann Rev Cell Dev Biol 2007;23:579–611. [PubMed: 17506703]

Hinshaw JE, Schmid SL. Dynamin self-assembles into rings suggesting a mechanism for coated vesicle budding. Nature 1995;374:190–192. [PubMed: 7877694]

Itoh T, Erdman KS, Roux A, Habermann B, Werner H, De Camilli P. Dynamin and the actin cytoskeleton cooperatively regulate plasma membrane invagination by BAR and F-BAR proteins. Dev Cell 2005;9:791–804. [PubMed: 16326391]

Kosaka T, Ikeda K. Possible temperature-dependent blockage of synaptic vesicle recycling induced by a single gene mutation in Drosophila. J Neurobiol 1983;14:207–225. [PubMed: 6304244]

Lee MC, Orci L, Hamamoto S, Futai E, Ravazzola M, Schekman R. Sar1p N-terminal helix initiates membrane curvature and completes the fission of a COPII vesicle. Cell 2005;122:605–617. [PubMed: 16122427]

Bielli A, Haney CJ, Gabreski G, Watkins SC, Bannykh SI, Aridor M. Regulation of Sar1 NH2 terminus by GTP binding and hydrolysis promotes membrane deformation to control COPII vesicle fission. J Cell Biol 2005;171:919–924. [PubMed: 16344311]

Lemmon MA. Membrane recognition by phospholipid-binding domains. Nat Rev Mol Cell Biol 2008;9:99–111. [PubMed: 18216767]

Leonard M, Song BD, Ramachandran R, Schmid SL. Robust colorimetric assays for dynamin's basal and stimulated GTPase activities. Methods Enzymol 2005;404:490–503. [PubMed: 16413294]

Marks B, Stowell MH, Vallis Y, Mills IG, Gibson A, Hopkins CR, McMahon HT. GTPase activity of dynamin and resulting conformation change are essential for endocytosis. Nature 2001;410:231–235. [PubMed: 11242086]

McIntyre JC, Sleight RG. Fluorescence assay for phospholipid membrane asymmetry. Biochemistry 1991;30:11819–11827. [PubMed: 1751498]

Merrifield CJ, Feldman ME, Wan L, Almers W. Imaging actin and dynamin recruitment during invagination of single clathrin-coated pits. Nat Cell Biol 2002;4:691–698. [PubMed: 12198492]

Miwako I, Schmid SL. Clathrin-coated vesicle formation from isolated plasma membranes. Methods Enzymol 2005;404:503–11. [PubMed: 16413295]

Ramachandran R, Schmid SL. Real-time detection reveals that effectors couple dynamin's GTP-dependent conformational changes to the membrane. EMBO J 2008;27:27–37. [PubMed: 18079695]

Ramachandran R, Surka M, Chappie JS, Fowler DM, Foss TR, Song BD, Schmid SL. The dynamin middle domain is critical for tetramerization and higher-order self-assembly. EMBO J 2007;26:559–566. [PubMed: 17170701]

Roux A, Uyhazi K, Frost A, De Camilli P. GTP-dependent twisting of dynamin implicates constriction and tension in membrane fission. Nature 2006;441:528–531. [PubMed: 16648839]

Sato K, Nakano A. Mechanisms of COPII vesicle formation and protein sorting. FEBS Lett 2007;581:2076–2082. [PubMed: 17316621]

Schmid SL, Smythe E. Stage-specific assays for coated pit formation and coated vesicle budding in vitro. J Cell Biol 1991;114:869–880. [PubMed: 1908470]

Shpetner HS, Vallee RB. Identification of dynamin, a novel mechanochemical enzyme that mediates interactions between microtubules. Cell 1989;59:421–432. [PubMed: 2529977]

Stowell MH, Marks B, Wigge P, McMahon HT. Nucleotide-dependent conformational changes in dynamin: evidence for a mechanochemical molecular spring. Nat Cell Biol 1999;1:27–32. [PubMed: 10559860]

Sweitzer SM, Hinshaw JE. Dynamin undergoes a GTP-dependent conformational change causing vesiculation. Cell 1998;93:1021–1029. [PubMed: 9635431]

Takei K, Haucke V, Slepnev V, Farsad K, Salazar M, Chen H, De Camilli P. Generation of coated intermediates of clathrin-mediated endocytosis on protein-free liposomes. Cell 1998;94:131–41. [PubMed: 9674434]

Warnock DE, Hinshaw JE, Schmid SL. Dynamin self-assembly stimulates its GTPase activity. J Biol Chem 1996;271:22310–22314. [PubMed: 8798389]

Yoshida Y, Kinuta M, Abe T, Liang S, Araki K, Cremona O, Di Paolo G, Moriyama Y, Yasuda T, De Camilli P, Takei K. The stimulatory action of amphiphysin on dynamin function is dependent on lipid bilayer curvature. EMBO J 2004;23:3483–3491. [PubMed: 15318165]

Zhang P, Hinshaw JE. Three-dimensional reconstruction of dynamin in the constricted state. Nat Cell Biol 2001;3:922–926. [PubMed: 11584275]

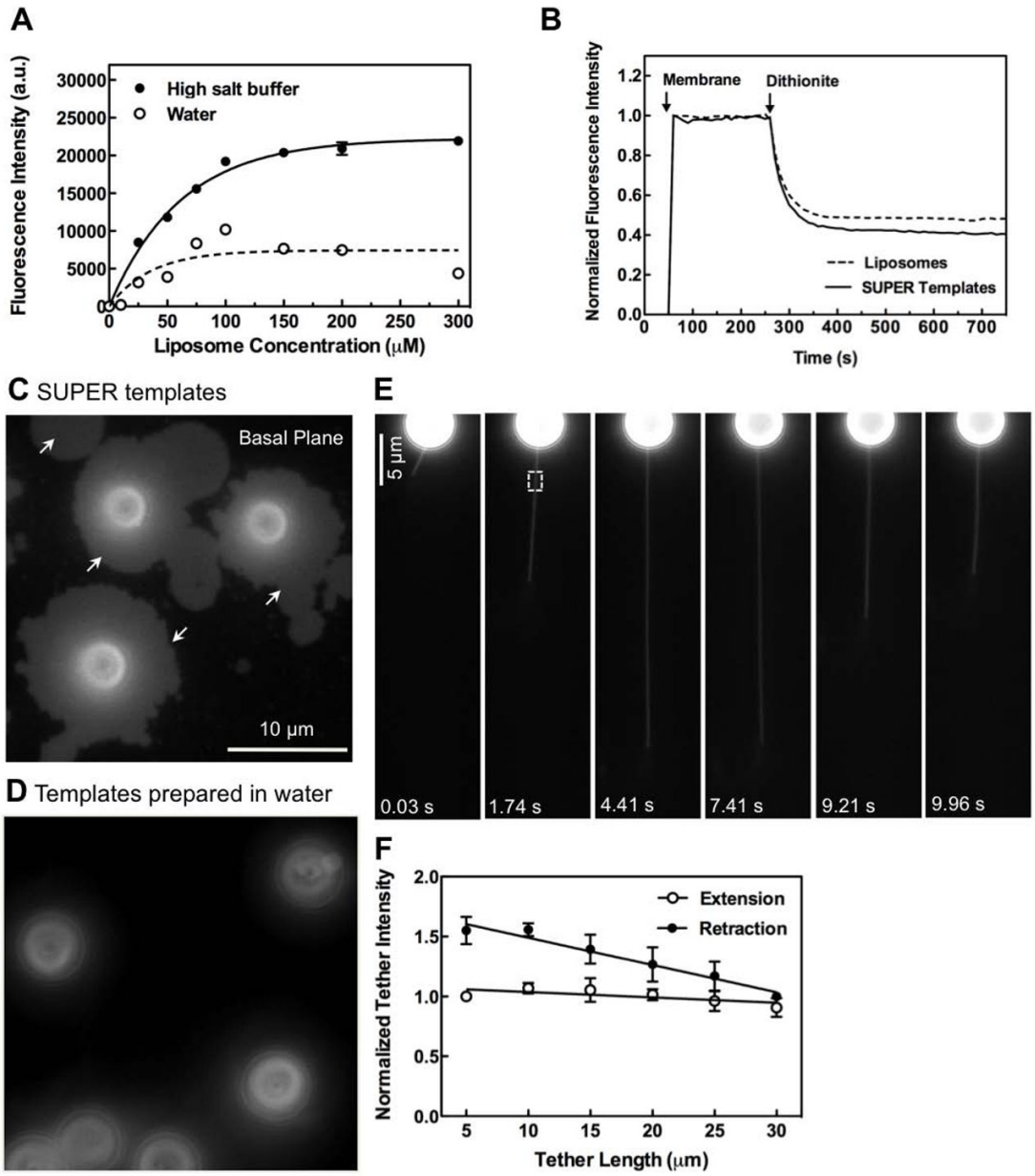

Figure 1. Supported bilayers with excess membrane reservoir (SUPER templates)

(A) Fluorescence intensity on silica beads incubated with increasing concentrations of DOPC:DOPS:PI-4,5-P_2:RhPE (79:15:5:1 mol%) liposomes in either 600 mM salt buffer or water and subsequently washed with water. Data represent the means±SD (n=3). (B) Dithionite-mediated quenching of fluorescence in DOPC:DOPS:PI-4,5-P_2:NBD-PE (78:15:5:2 mol%) liposomes and SUPER templates formed from these liposomes. Plots are the mean of n=5 independent fluorescence intensity traces. Fluorescence images of (C) SUPER templates (see Movie S1) and (D) templates prepared in water added to a glass coverslip. (E) Extension and retraction of a membrane tether from a SUPER template (see Movie S2). (F) Fluorescence intensities in the ROI in (E, white square) plotted as a function of tether length. Data in extension plots are normalized to the tether intensity at 5 μm and in retraction plots to tether intensity at 30 μm. Data represent the mean±SD (n=5).

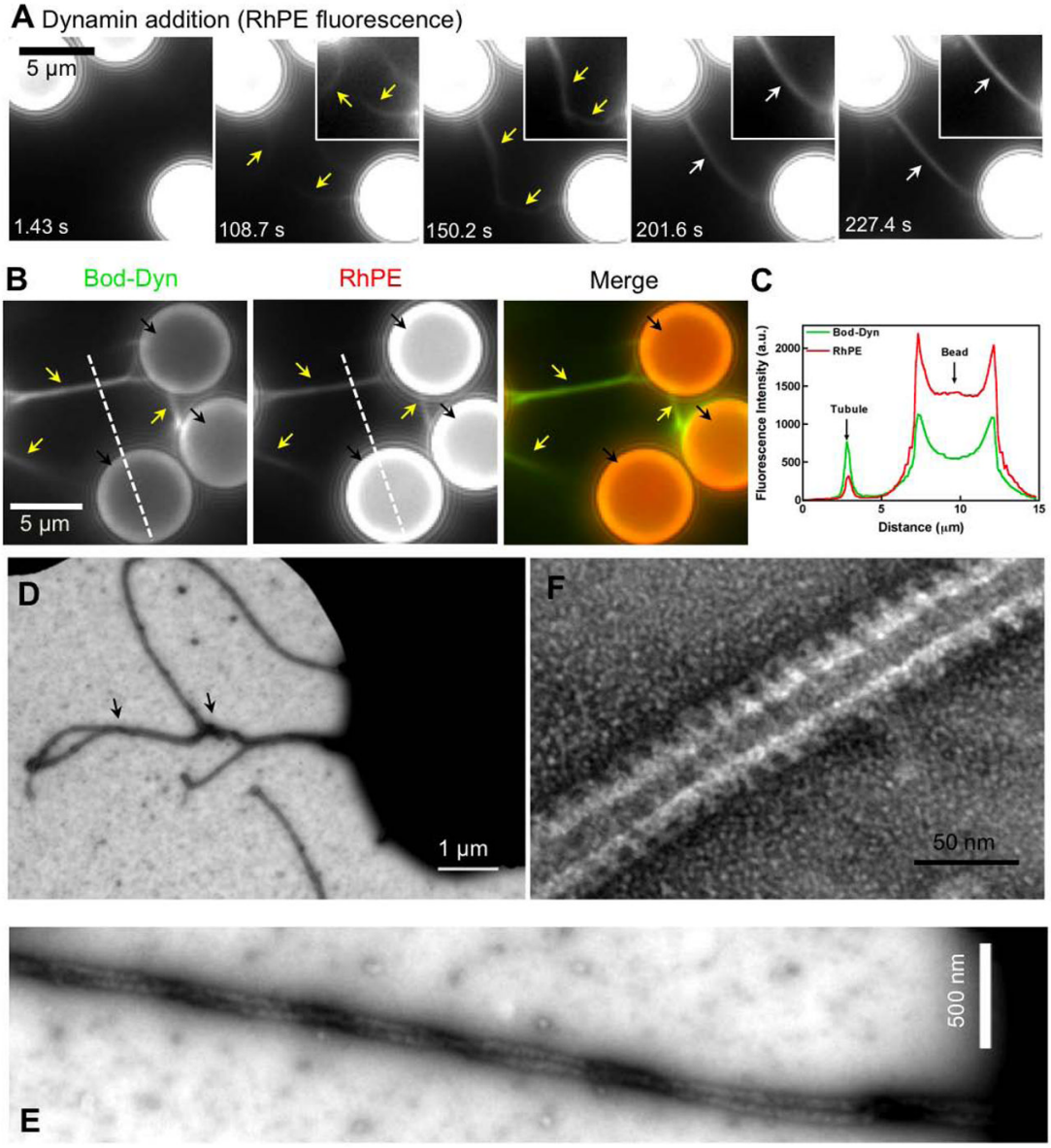

Figure 2. Dynamin-induced membrane tubulation from SUPER templates

(A) Time-lapse images showing the effect of adding dynamin to templates. See Movie S3. Insets are relevant portions in respective frames adjusted for contrast. (B) Fluorescence of BODIPY-dynamin (Bod-Dyn) and membrane (RhPE) on membrane tubules and SUPER templates. (C) Fluorescence intensity across the dotted line shown in (B). Negative-stain EM of a dynamin-coated coiled membrane tubule at low (D) and high (E) magnification. (F) Negative-stain EM showing the dynamin scaffold on an individual membrane tubule.

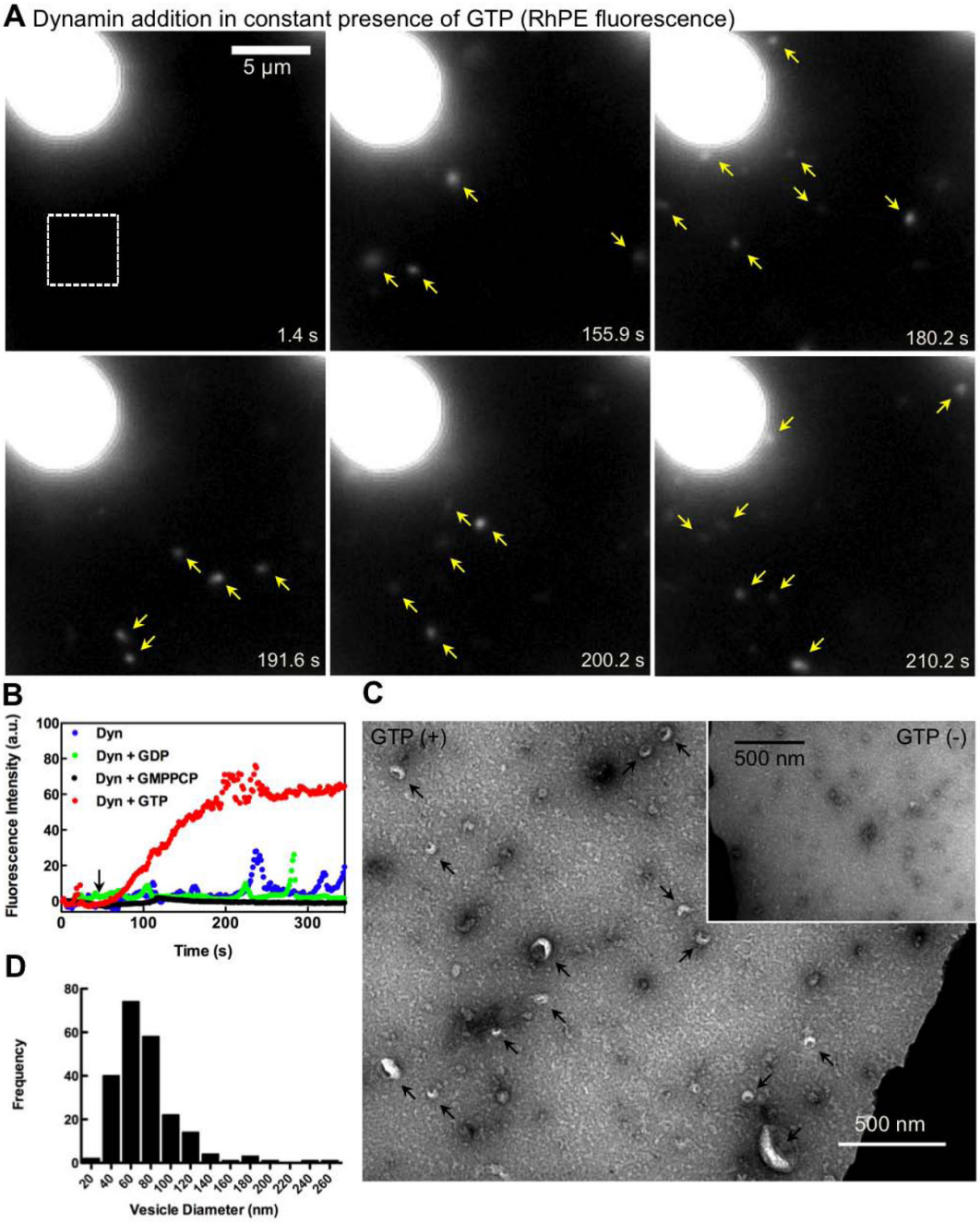

Figure 3. Dynamin-catalyzed membrane fission leading to vesicle release

(A) Time-lapse images showing the effect of adding dynamin to SUPER templates in the presence of GTP (see Movie S4). (B) Mean fluorescence intensities in a small area of the bathing solution (white square in A) monitored after dynamin addition to templates in buffer alone or with GMPPCP, GDP, or GTP. Black arrow marks dynamin addition. (C) Negative-stain EM of the bathing solution after adding dynamin and GTP to templates. Inset shows a negative-stain EM of the bathing solution after adding dynamin to templates in the absence of GTP. (D) Size distribution of vesicles (n=221) measured from EM micrographs.

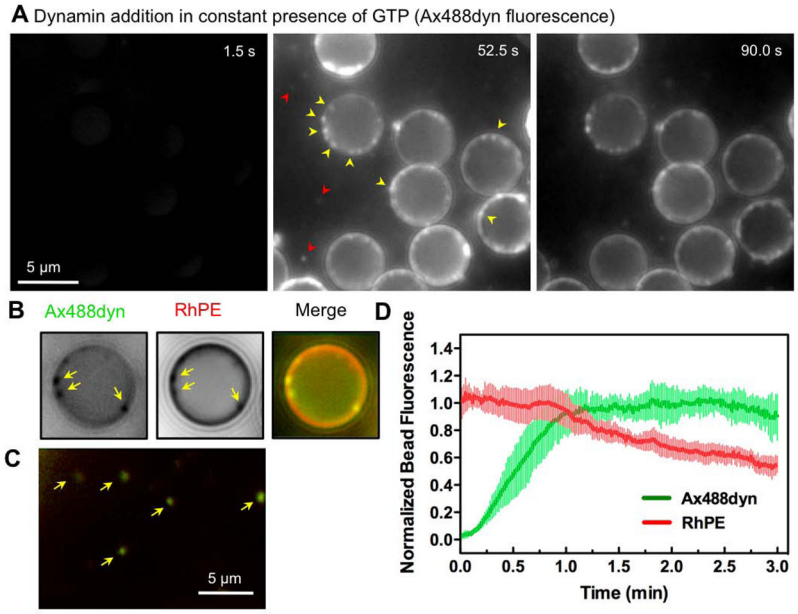

Figure 4. Dynamin behavior during membrane fission

(A) Time-lapse images showing the effect of adding Ax488dyn to templates in presence of GTP (see Movie S5). (B) Colocalization of punctate Ax488dyn fluorescence on the template with high RhPE fluorescence in presence of GTP. Ax488dyn and RhPE images are inverted in contrast for clarity. (C) Colocalization of Ax488dyn and RhPE fluorescence in the bathing solution in the presence of GTP. (D) Plots showing background corrected Ax488dyn and RhPE fluorescence on templates in the presence of GTP. Data represents the mean±SD (n=8).

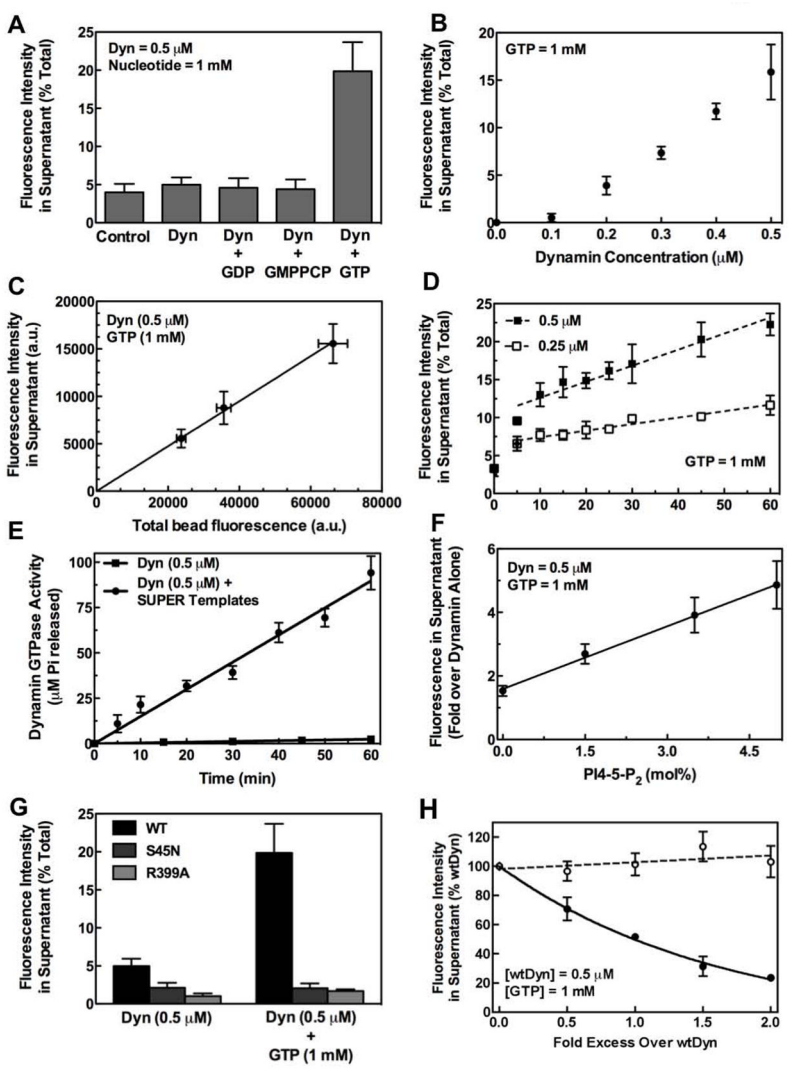

Figure 5. Biochemical analysis of membrane fission by sedimentation assays

(A) Nucleotide dependence for dynamin-catalyzed membrane fission. (B) Dependence of membrane fission on dynamin concentration. Data are corrected for background fluorescence in the supernatant of control samples. (C) Dependence of membrane fission on concentration of SUPER templates. Data are corrected for background fluorescence in the supernatant of control samples. (D) Dependence of fission kinetics on dynamin concentration. (E) Dynamin GTPase activity in the presence and absence of SUPER templates. (F) Dependence of fission on PI-4,5-P_2 concentration in the membrane. Data are normalized to fluorescence in supernatant of samples with dynamin alone. (G) Comparison of membrane fission with wild type (WT), GTP-binding defective (S45N), and self-assembly defective (R399A) dynamin. (H) Effect of increasing concentrations of S45N (filled circles) and R399A (open circles) on WT dynamin-catalyzed membrane fission. In all cases, dynamin and nucleotides were premixed in solution before addition of templates. All data represent the mean±SD (n≥3).

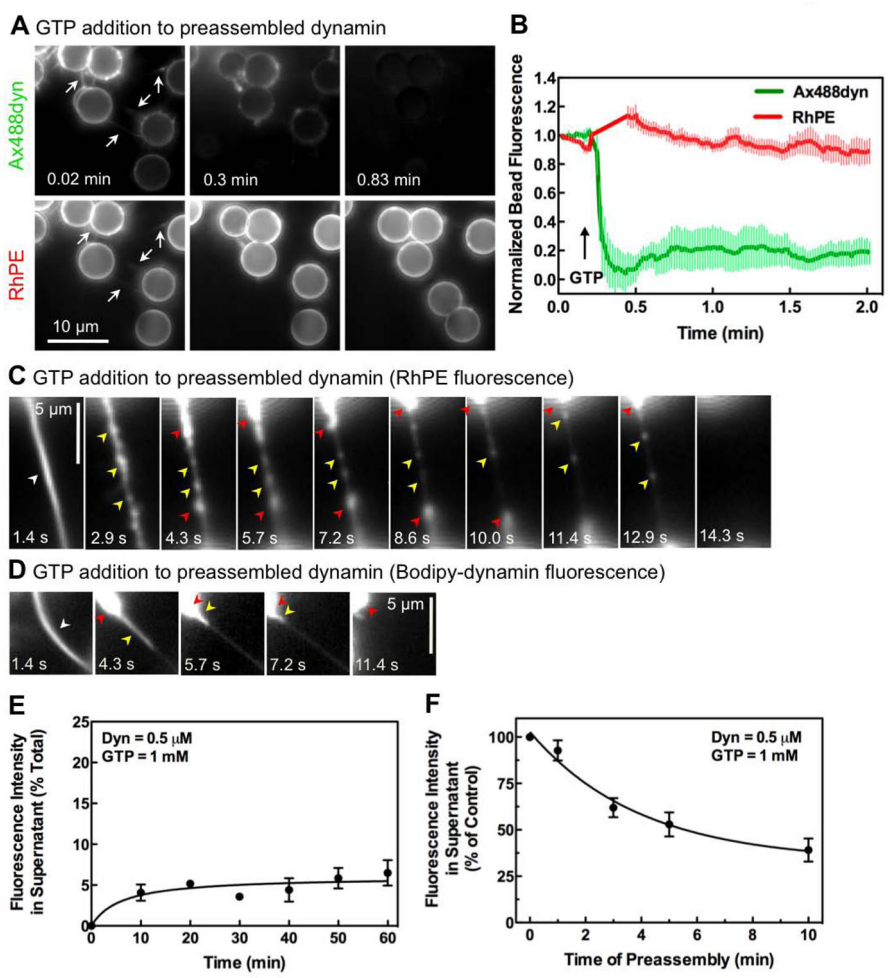

Figure 6. Behavior of preassembled dynamin in response to GTP addition

(A) Time-lapse images showing the effect of GTP addition to an apparent network of bundled membrane tubules of preassembled dynamin (see Movie S8). (B) Plots showing background corrected Ax488dyn and RhPE fluorescence on templates before and after GTP addition. Data represent the mean±SD (n=8). (C) Time-lapse images showing the effect of GTP addition to dynamin-coated bundled membrane tubules tethered between templates (see Movie S9). (D) Time-lapse images showing the effect of GTP addition to preassembled BODIPY-dynamin on bundled membrane tubules tethered between templates (see Movie S10). (E) Dynamin-catalyzed membrane fission after dynamin preassembly. Dynamin was preassembled on SUPER templates for 10 min before GTP addition. Data are corrected for background fluorescence in supernatant from control samples. (F) Dependence of extent of fission on the duration for which dynamin is preassembled on the template. All data represent the mean±SD (n≥3).

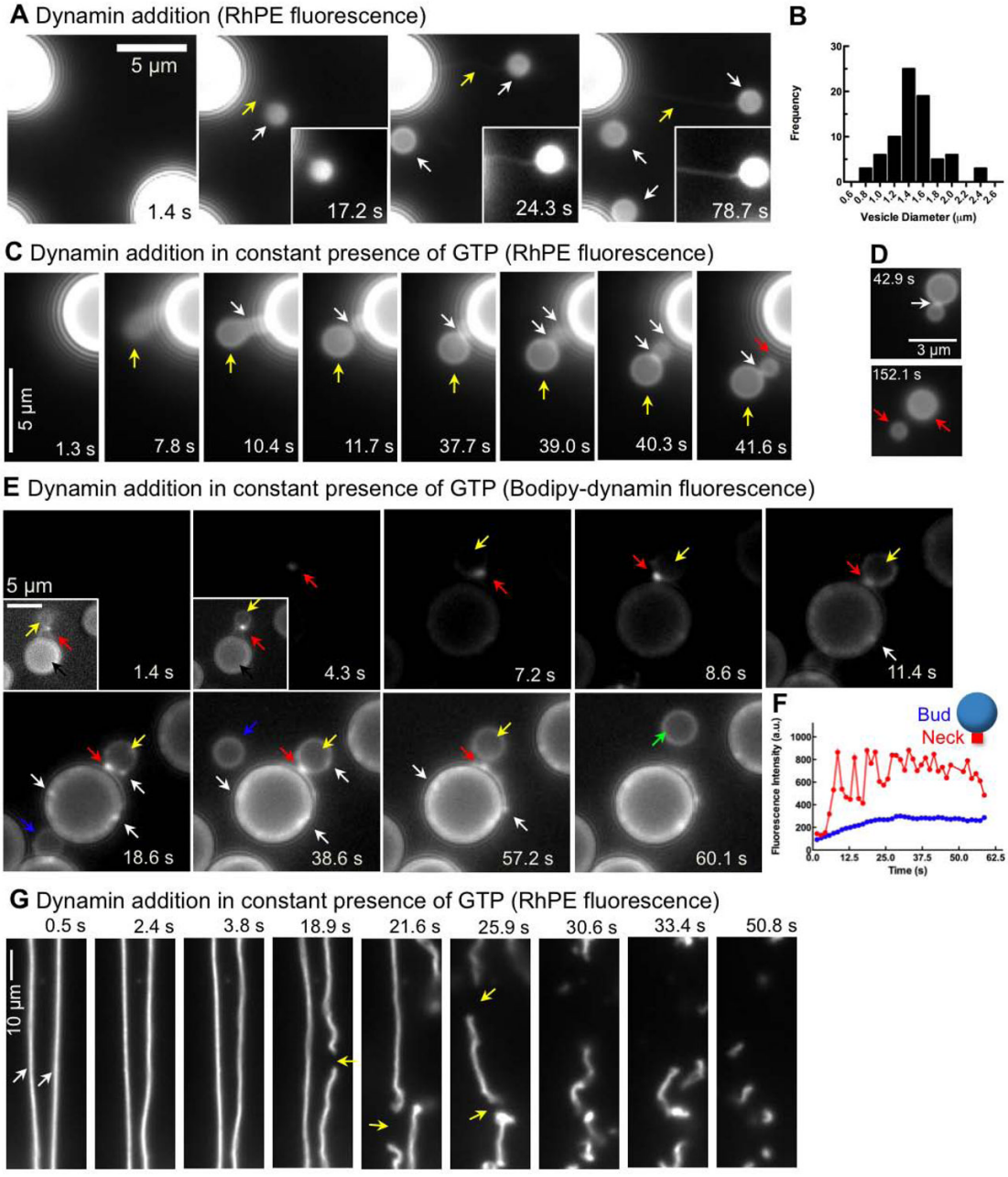

Figure 7. Visualizing dynamin-catalyzed membrane fission

(A) Time-lapse images showing the effect of adding dynamin suspended in glycerol (final dynamin concentration=0.5 μM, final glycerol concentration=2%) to SUPER templates. Insets are relevant portions in respective frames adjusted for contrast. See Movie S12. (B) Size distribution of buds (n=77) measured from fluorescence micrographs. (C) Time-lapse images showing the effect of adding dynamin suspended in glycerol to templates in the presence of GTP (see Movie S13). (D) Time-lapse images showing the effect of dynamin on a membrane template of conjoined buds in the presence of GTP (see Movie S14). (E) Time-lapse images showing the effect of adding BODIPY-dynamin suspended in glycerol to templates in the presence of GTP. Insets in the first two frames are relevant portions in respective frames adjusted for contrast. See Movie S15. (F) Plots showing fluorescence of BODIPY-dynamin at

the neck (red trace) and the bud (blue trace) during a fission event of the large bud shown in (E). (G) Time-lapse images showing the effect of adding dynamin to a membrane template of partially retracted membrane tethers generated from SUPER templates in the presence of GTP (see Movie S16).